

## HRTEM, XPS and XRD characterization of ZnS/PbS nanorods prepared by thermal evaporation technique

B. Abadllah<sup>\*,1</sup>, B. Assfour<sup>2</sup>, M. Kakhia<sup>1</sup>, Ali Bumajdad<sup>3</sup>

<sup>1</sup>Atomic Energy Commission, Department of Physics. P. O. Box 6091, Damascus, Syria

<sup>2</sup>Atomic Energy Commission, Department of chemistry. P. O. Box 6091, Damascus, Syria

<sup>3</sup>Chemistry Department, Faculty of Science, Kuwait University, Safat 13060, Kuwait

\*pscientific27@aec.org.sy

PACS 61.46.+w

DOI 10.17586/2220-8054-2020-11-5-537-545

Zinc sulfide (ZnS) and zinc sulfide/lead sulfide (ZnS/PbS) nanorods were grown on glass substrates using a thermal evaporation method. The morphology of the prepared samples has been studied by transmission electron microscopy (TEM), field-emission scanning electron microscopy (FE-SEM) and Scanning Electron Microscopy (SEM). Both differences and similarities in morphology between the samples have been discovered. In the ZnS/PbS sample, ZnS nanorods were formed with diameter less than 50 nm and length between 2000 and 3000 nm. The pure ZnS sample has dense structure and its thickness was about 200 nm. Samples were studied in detail using energy-dispersive X-ray spectroscopy (EDX). The surface chemical compositions of the samples were confirmed by means of X-ray photoelectron spectroscopy (XPS). The determination of the crystal structure using the X-ray diffraction revealed that two phases of ZnS, blende and wurtzite, are present in the sample after adding Pb, while only blende is identified in the pure ZnS sample.

**Keywords:** nanorods, ZnS, HRTEM, XPS, thermal evaporation.

*Received:* 1 September 2020

*Revised:* 28 September 2020

### 1. Introduction

ZnS, ZnO, AlN and CN<sub>x</sub> nanotubes are envisaged to be highly promising for applications in semiconductors, photo detectors, lasers, solar cells, and -nanogenerators [1]. During the last decade zinc sulfide (ZnS) has been categorized as one of the most propitious semiconductor materials due to its wide device applications [2–8]. It is environmentally friendly, cheap and easy to prepare. The potential application of ZnS in solar cell applications is well established [9]. As is used as a buffer layer, the spectral response of the solar cell is increased. ZnS is a polymorphic solid, meaning it has the ability to exist in more than one crystal structure. It has a direct wide band gap of 3.2–3.9 eV at room temperature [10]. It appears as cubic (known zinc blende or sphalerite) or as a hexagonal wurtzite structure (Fig. 1). The blende form is the most common natural form of ZnS and it is almost identical to the Si unit cell with a band gap of 3.7 eV.

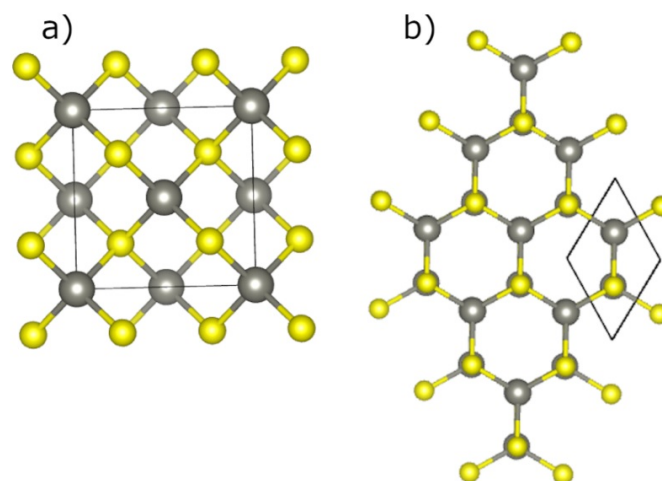


FIG. 1. The cubic unit cell of zinc blende (a) and the hexagonal unit cell of wurtzite (b). Sulfur and zinc atoms are represented as yellow and gray spheres, respectively

Several methods have been used to prepare ZnS films by different research groups [11], such as magnetron sputtering [12, 13], pulsed laser deposition, chemical bath deposition (CBD) [14], ultrasonic spray pyrolysis [15], electron gun evaporation [16] and thermal evaporation [12]. The latter is particularly interesting, due to its simplicity and cheapness. Moreover, thermal evaporation process produce polycrystalline material with a predominant cubic phase [12]. ZnS deposition on different substrates, such as silicon, glass, and titanium oxide, have been also extensively discussed in the literature [17, 18]. It is well established that the substrate plays a crucial role in determining the quality of the deposited sample. For example, depending on the crystalline quality of the AlN substrate ZnO deposited films show an epitaxial growth [19, 20]. Extensive studies have been reported on ZnS nanostructures doped with different transition metal ions (such as Co, Mn, Ni, Fe) prepared by different techniques [21–24]. Depending on the type of dopant ion, the doped materials exhibit different luminescent, electronic and magnetic properties.

In this work, we prepare a ZnS/PbS nanostructures deposited on glass substrates using a vacuum-based simple thermal evaporation method. Several characterizations techniques were applied to describe their morphology, composition and structural properties. HRTEM and SEM techniques were applied to investigate the morphology of samples. The crystallographic properties of the films were studied using X-ray diffraction method. EDX and XPS scans are used for quantification of Zn, S and Pb in the sample.

## 2. Experimental methods

ZnS/PbS thin films were prepared on glass substrates using simple thermal evaporation technique. 12 wt% PbS powder is added to 88 wt% ZnS powder (99.99% purity) in the crucible as source material, under a vacuum of  $10^{-5}$  Torr using low speed turbomolecular pump (pumping speed 25000 rpm). The chamber geometry, gas flow and the gas remaining time enhance the thin film quality [25]. The distance between the ZnS and substrate holder was about 25 cm; the substrate holder was heated before deposition to 100 °C. Thin film morphology was examined using scanning SEM, TSCAN Vega\XMU model, equipped with energy dispersive spectroscopy (EDX) to determine the chemical composition of the synthesized films. Transmission electron microscopy (TEM) images for ZnS/PbS sample were also taken to verify the film morphology. The X-ray diffraction (XRD) measurements were carried out on uncompressed powder inside steel holder by using Bruker, D8 ADVANCE diffractometer with Cu  $K\alpha$  ( $\lambda = 0.154$  nm), measurements were conducted in the range of 20–80° ( $2\theta$ ). Phase identification from powder diffraction data was performed using the QualX peaks identification software [26]. The diffraction data was further analyzed using Rietveld refinements method as implemented in GSAS-II package [27].

The XPS experiments were performed using a model VG Scientific 200 spectrometer (UK) equipped with MgK $\alpha$  radiation (1253 eV) and operated at 23 kV and 13 mA. All binding energy values (in eV) were determined with respect to the C1s line (284.6 eV).

TEM was performed with a JEM2200FS double aberration-corrected transmission electron microscope (JEOL Ltd.) which was operating at an acceleration voltage of 200 kV.

## 3. Results and dissection

The chemical composition of the film deposited on the glass substrate was explored by means of EDX and XPS techniques. Fig. 2 shows the collected EDX spectrum of the products. Spectrum analysis shows that the film is composed of Zn, Pb, S and small amount of C and O elements (Table 1). The concentration of S in the sample is almost equal to the sum of Zn and Pb concentrations ( $S/(Zn+Pb) = 0.998$ ). The C and O atoms are contaminants from the atmosphere which are extremely difficult to avoid. Hence, our product is a stoichiometric film. Films with same stoichiometry were also acquired by different techniques, such as ultrasonic spray pyrolysis [15] and electron beam evaporation [16].

TABLE 1. Atomic percentage for Zn, Pb, S, O and C elements from EDX analysis

Element	Weight %	Atomic %
C_K	1.9	7.4
O_K	0.03	0.08
S_K	31.96	46.72
Pb_M	3.25	0.74
Zn_K	62.86	45.07

For further investigation of the chemical composition of the product, XPS scan of the sample was performed (Fig. 3). In order to compensate the surface charging effects C 1s signal (284.6 eV) was used as a reference signal.

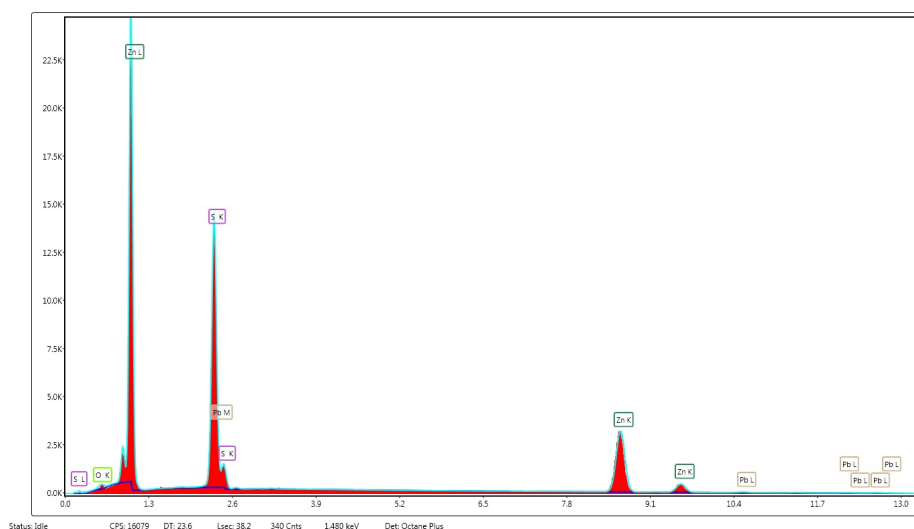


FIG. 2. EDX spectrum for ZnS/PbS nanorods films deposited on glass substrate

XPS curves were fitted (lowest curve in each spectrum) after adjusting to theoretical curves. Detailed spectra for the Zn2p, S2p, Pb4f, regions and related data are presented in Fig. 4. The results of XPS surface analyses are summarized in Table 2, which confirm the formation of ZnS and PbS compound and the stoichiometry of the film. Moreover, there was a strong indication for the presence of traces of, ZnO, PbO, CO and PbSO<sub>3</sub> on the surface of the films due to preparation and measurement conditions.

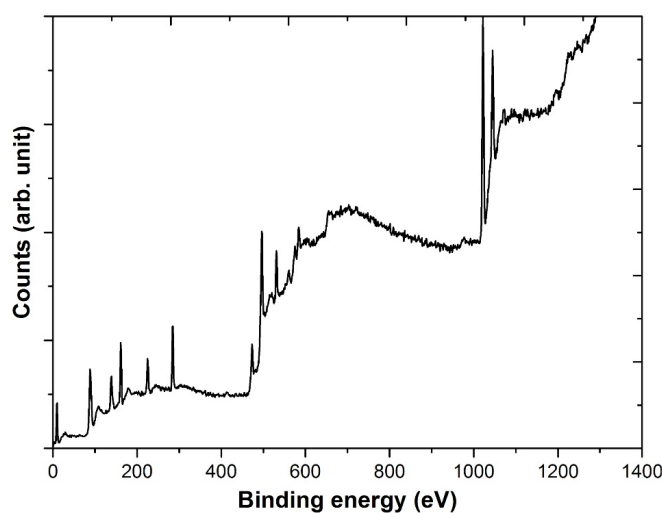


FIG. 3. XPS scans of ZnS/PbS sample on glass substrate

The X-ray diffraction pattern of the pure ZnS sample at room temperature is shown in Fig. 5. The peaks can be tied to the blend phase of ZnS. A good agreement between observed and calculated spectra was obtained; typical  $wR_p$  of the fit was  $\sim 0.09$ . For the ZnS/PbS product, the best agreement between observed and calculated pattern could only be achieved by the presence of the two phases of ZnS (blende and wurtzite) and one phase for PbS, namely galena (Fig. 6). The phase fraction for each identified phase in the product was fitted simultaneously. Indications from XRD results show that the ZnS/PbS sample contains more zinc blende (23.42%) than wurtzite (9.53%). The concentration of the PbS phase is 3.32% and the rest is SiO<sub>2</sub>. The ratio between the PbS phase and ZnS phases is about 0.1 which coincide with the XPS results. X-ray line width measurements have shown that the average particle size of ZnS is about 30 nm. The average strain value was found to be negligible for all phases. Such low value of strain is advantageous because the films have a good adhesion without high stress value. This can be attributed to the thermal evaporation technique. These results were in agreement with work of Benyahia *et al.* [11], where thermal evaporation was also

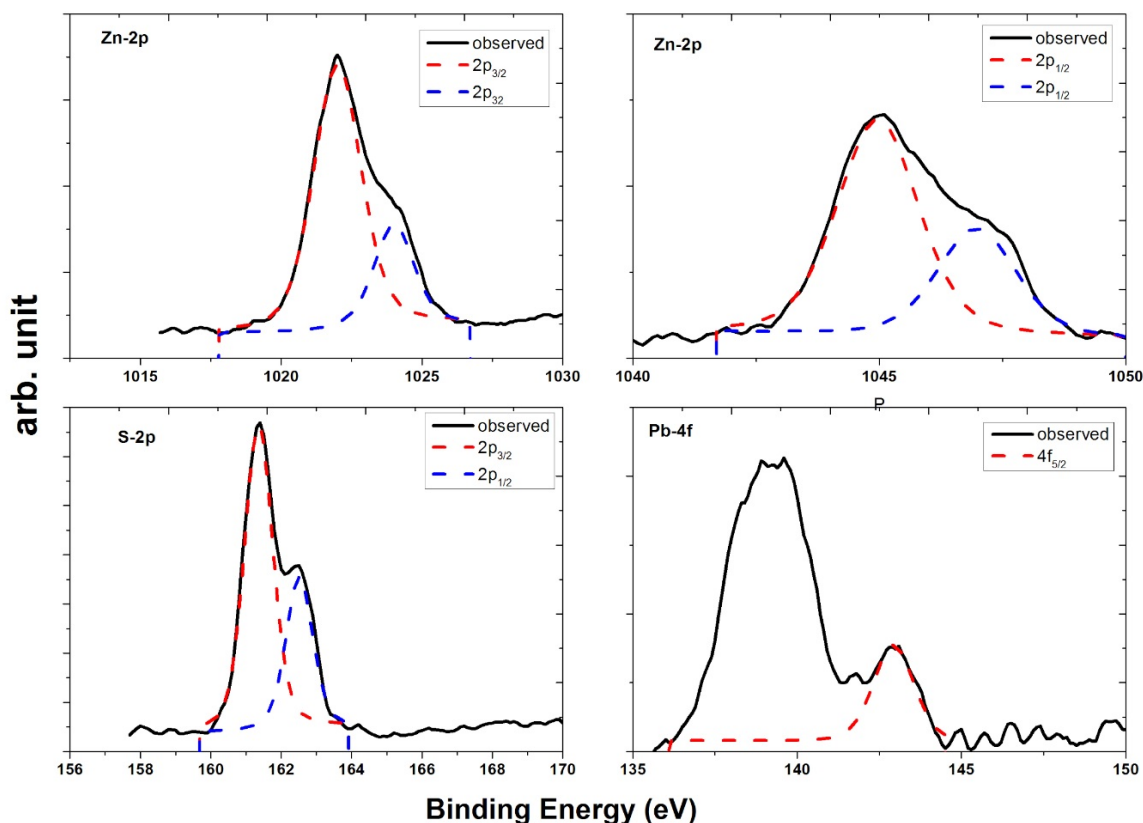


FIG. 4. Zn2p, S2p and Pb 4f XPS spectra recorded for the ZnS/PbS sample. Photon energies are 1253 eV

TABLE 2. XPS spectral features table

Name	Peak BE/eV	FWHM/eV	Area (P) CPS/eV	Atomic %	Peak assignment
C1s	284.7	1.0	1174.9	21.4	(C–C) adventitious carbon
C1s A	285.2	1.2	1216.2	22.2	(C–O–C) adventitious carbon
C1s B	288.4	1.2	127.9	2.3	(O–C=O) adventitious carbon
O1s	531.3	1.4	922.2	6.7	(Organic C=O) chemisorbed oxygen[28,29]
O1s A	532.1	1.8	793.6	5.8	(Organic C–O) chemisorbed oxygen
Pb4f, 5/2	142.9	1.5	247.8	0.2	Pb in PbS[30, 31]
Pb4f, 7/2	138.2–139.6	1.2	13038.4	0.5	Pb in Pb(OH) <sub>2</sub> / PbO/PbSO <sub>4</sub>
Zn2p, 3/2	1022.0	2.0	7296.1	10.6	Zn in ZnS/ ZnO
Zn2p, 3/2 A	1024.0	1.7	2289.3	3.3	Zn in ZnS[32, 33]
Zn2p, 1/2	1045.0	2.0	2915.9	4.3	Zn in ZnS[34, 35]
Zn2p, 1/2 A	1047.0	1.9	1408.3	2.1	Zn in ZnS
S2p, 3/2	161.4	1.0	1404.5	14.3	Sulphur in metal sulfide
S2p, 1/2	162.5	0.9	662.9	6.8	Sulphur in S–O/S–C/S–H

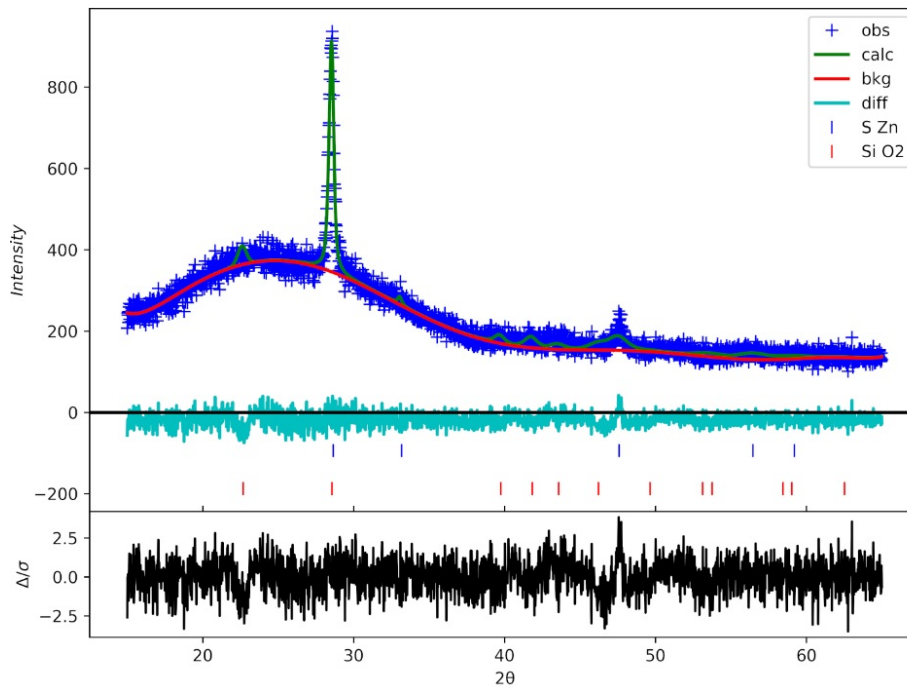


FIG. 5. X-ray diffraction data acquired from pure ZnS sample (blue +) including Rietveld refinements (green line) and background (red line). Vertical dashed lines denote  $d_{hkl}$  values associated with ZnS and SiO<sub>2</sub> phases

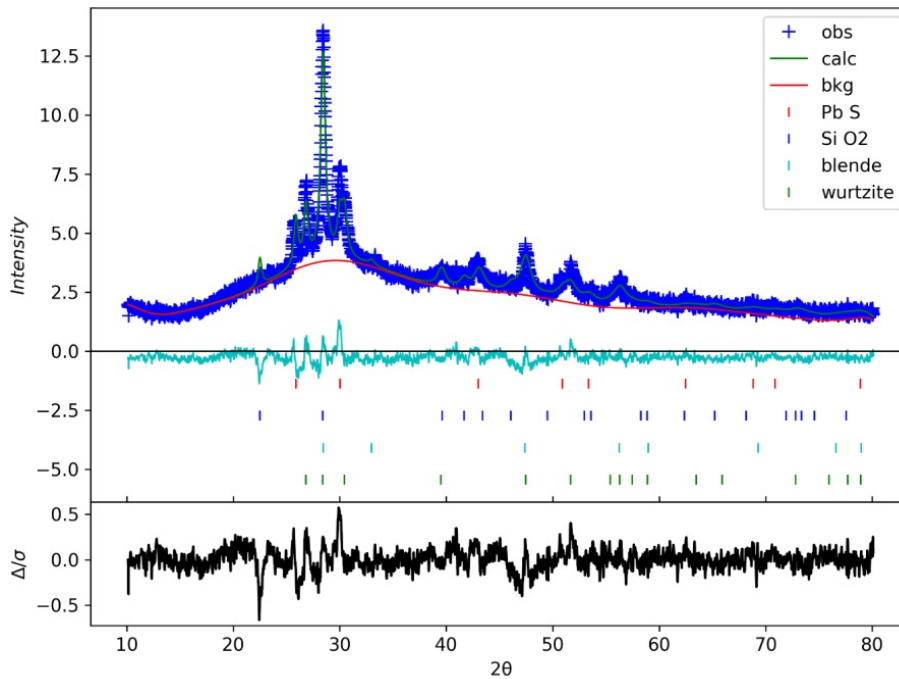


FIG. 6. X-ray diffraction data acquired from ZnS/PbS sample (blue +) including Rietveld refinements (green line) and background (red line). Vertical dashed lines denote  $d_{hkl}$  values associated with ZnS (two phases), PbS and SiO<sub>2</sub> phases. Typical  $wR_p$  of the fit is  $\sim 0.07$

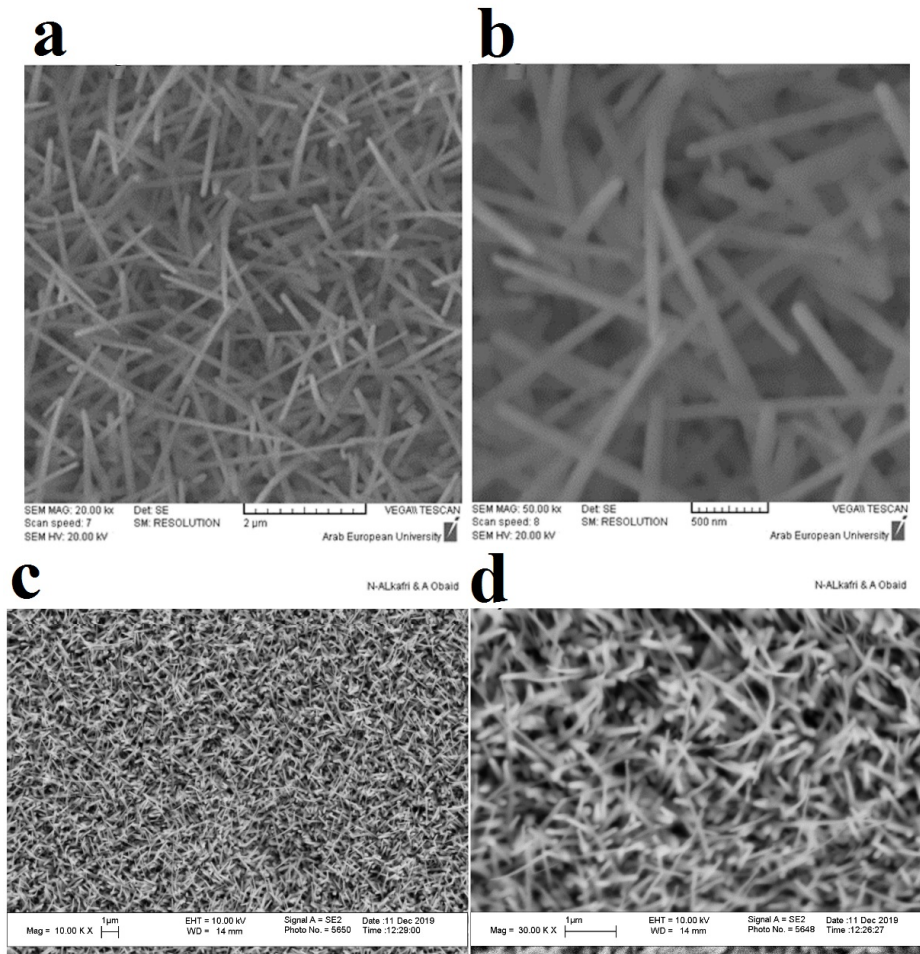


FIG. 7. SEM images in low (a) and high (b) magnification. FE-SEM in low (c) and high (d) magnification for the ZnS/PbS nanorods grown on glass templates

used for ZnS deposition and blende structure was obtained. The blende structure was also obtained in our previous work, where deposition was performed using electron gun techniques [16]. The identified PbS phase, galena, has also a cubic structure. Galena is a natural mineral of Pb, it is most abundant sulfide minerals and mostly associate with blende and calcite minerals. Therefore, the presence of the Zn blende and Pb galena together in the same thin film is not surprising. It worth mentioning that, unlike previously reported work on the growth of wurtzite ZnS nanorods [36], no phase transformation from zinc blende to wurtzite ZnS has been observed in the present product. It is clear in fact that the addition of increased amounts of lead to the compound (ZnS) of the amphoteric element (Zn) will generally result in a greater ionic character of the chemical bond between the “cation” and “anion”. It is well known, that blende (ZB) is a lattice with a less ionic bond. While, wurtzite (WZ) with a more ionic bond [37], therefore the high bond polarity favors the wurtzite structure instead of zinc-blende structure and the appearance of a wurtzite structure in our sample is in full agreement with the known general chemical concepts. A number of authors have recognized the effect of growth parameters such as substrate temperature and the ratio of dopant atoms on phase formation. For example, Karan *et al.* reported about the reversible phase transformation of platelet-shaped ZnS nanostructures between e (WZ) and (ZB) phases by reversible insertion/ejection of dopant Mn(II) ions induced by a thermocyclic process [38]. Joyce *et al.* showed that simply by tailoring the basic growth parameters of temperature and V-III ratio, pure ZB and pure WZ III-V nanowires can be obtained [39]. Amico and coworker investigated doping effects, as induced by Al and Cu, on promoting different ZnS phases using first principles simulations [40].

SEM is a versatile tool to investigate the surface topography and features of nanostructured materials. Moreover, it is useful to determine the growth mode of deposited films. Fig. 7(a,b) shows the SEM plane-view images of the ZnS/PbS sample in two different magnifications. It is clear that the template substrate covered with ZnS nanorods. This confirms the growth as nanorods for ZnS deposited on glass substrate. FESEM (Fig. 7(c,d)) scan shows similar

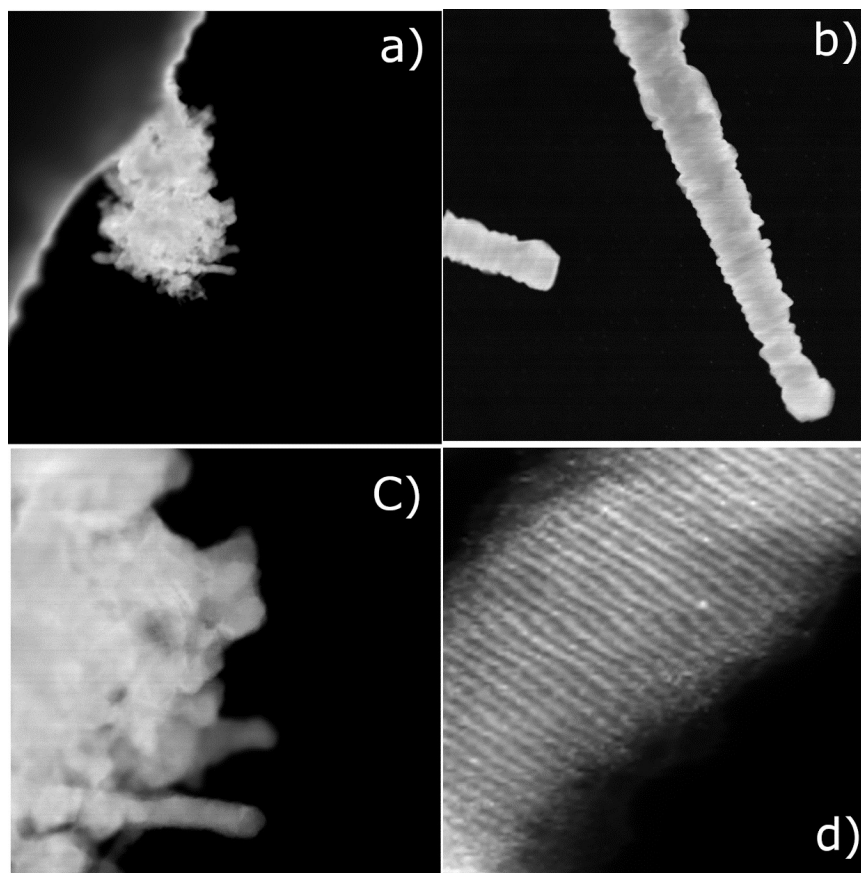


FIG. 8. (a and b) TEM morphology image of the synthesized ZnS/PbS nanorods. (c) TEM image of an individual nanorod. (d) HRTEM image of one selected nanorod

images for the surface morphology of the sample. The growth mechanism for the ZnS nanorods can be explained as following: the PbS evaporated initially because of the temperature milting (evaporation temperature of PbS is lower than of ZnS), and it formed monolayer or nucleation layer. Moreover, the growth of objects is enhanced as large lead atoms acting as dopants markedly accelerate the diffusion processes.

For further investigation of the film morphology, TEM and HRTEM characterization of the sample were performed. Although the TEM has many advantages over SEM, it has also some drawback and limitations. For example, sample preparation is much more difficult than SEM and results from TEM scan are dependent on the quality and cleanliness of the sample. Fig. 8 gives a TEM morphology image of the sample in low and high magnifications. Fig. 8(c) shows the TEM image of an individual nanorod, revealing the flat and smooth surface with uniform diameters of the nanorod. The mean value of nanorod is varying between 180 and 200 nm. Fig. 8(d) shows the HRTEM image of one nanorod in the lattice fringes.

#### 4. Conclusions

In summary, we prepared ZnS/PbS nanorods deposited on substrate of glass using thermal evaporation technique. SEM and TEM images are used for exploring morphology of the films. They confirm the formation of nanorods with a mean diameter 200 nm. Chemical composition of the product was investigated by mean of EDX and XPS. it confirms the stoichiometry of the film. XRD pattern analysis indicates the presence of two phase from ZnS (blende and wurzite) and one phase from PbS (galena).

#### Acknowledgements

The authors greatly acknowledge support to this project by Professor I. Othman, the Director General of the Atomic Energy Commission of Syria. Prof. Dr. Toma Susi for HRTEM measurement. The Kuwait University Research Administration, under Grant Number's GS 01/05 and GS 03/01 for XPS and XRD analysis. The Nanoscopy Science Center at Kuwait University for performing FESEM measurement.

## References

- [1] Huang X., Wang M., Willinger M.-G., Shao L., Su D.S., Meng X.-M. Assembly of Three-Dimensional Hetero-Epitaxial ZnO/ZnS Core/Shell Nanorod and Single Crystalline Hollow ZnS Nanotube Arrays. *ACS Nano*, 2012, **6**(8), P. 7333-9.
- [2] Leftheriotis G., Papaefthimiou S., Yianoulis P. Integrated low-emittance-electrochromic devices incorporating ZnS/Ag/ZnS coatings as transparent conductors. *Solar Energy Materials and Solar Cells*, 2000, **61**(2), P. 107-12.
- [3] Kavanagh Y., Alam M.J., Cameron D.C. The characteristics of thin film electroluminescent displays produced using sol-gel produced tantalum pentoxide and zinc sulfide. *Thin Solid Films*, 2004, **447-448**, P. 85-9.
- [4] Wan H., Xu L., Huang W.-Q., Huang G.-F., He C.-N., Zhou J.-H., et al. Band engineering of ZnS by codoping for visible-light photocatalysis. *Applied Physics A*, 2014, **116**(2), P. 741-50.
- [5] Nizamoglu S., Ozel T., Sari E., Demir H.V. White light generation using CdSe/ZnS core-shell nanocrystals hybridized with InGaN/GaN light emitting diodes. *Nanotechnology*, 2007, **18**(6), P. 065709.
- [6] Bae W.K., Kwak J., Park J.W., Char K., Lee C., Lee S. Highly Efficient Green-Light-Emitting Diodes Based on CdSe@ZnS Quantum Dots with a Chemical-Composition Gradient. *Advanced Materials*, 2009, **21**(17), P. 1690-4.
- [7] Wang L., He W., Xiao X., Meng F., Zhang Y., Yang P., et al. Hysteresis-Free Blue Phase Liquid-Crystal-Stabilized by ZnS Nanoparticles. *Small*, 2012, **8**(14), P. 2189-93.
- [8] Samadpour M. Efficient CdS/CdSe/ZnS quantum dot sensitized solar cells prepared by ZnS treatment from methanol solvent. *Solar Energy*, 2017, **144**, P. 63-70.
- [9] Diamond A.M., Corbellini L., Balasubramaniam K.R., Chen S., Wang S., Matthews T.S., et al. Copper-alloyed ZnS as a p-type transparent conducting material. *Physica status solidi(a)*, 2012, **209**(11), P. 2101-7.
- [10] Shin S.W., Pawar S.M., Park C.Y., Yun J.H., Moon J.-H., Kim J.H., et al. Studies on Cu<sub>2</sub>ZnSnS<sub>4</sub> (CZTS) absorber layer using different stacking orders in precursor thin films. *Solar Energy Materials and Solar Cells*, 2011, **95**(12), P. 3202-6.
- [11] Benyahia K., Benhaya A., Aida M.S. ZnS thin films deposition by thermal evaporation for photovoltaic applications. *Journal of Semiconductors*, 2015, **36**(10), P. 103001.
- [12] Haque F., Rahman K.S., Islam M.A., Chelvanathan P., Chowdhury T.H., Alam M.M., et al., editors. A Comparative Study on ZnS Thin Films Grown by Thermal Evaporation and Magnetron Sputtering. IEEE Student Conference on Research and Development (SCOReD), 16-17 December, 2013, Putrajaya, Malaysia.
- [13] Jazmati A.K., Abdallah B., Lahlah F., Shaker S.A. Photoluminescence and optical response of ZnO films deposited on silicon and glass substrates. 2019.
- [14] Abdallah B., Ismail A., Kashoua H., Zetoun W. Effects of Deposition Time on the Morphology, Structure, and Optical Properties of PbS Thin Films Prepared by Chemical Bath Deposition. *Journal of Nanomaterials*, 2018, **2018**, P. 8.
- [15] Alnama K., Abdallah B., Kanaan S. Deposition of ZnS thin film by ultrasonic spray pyrolysis: effect of thickness on the crystallographic and electrical properties. *Composite Interfaces*, 2017, **24**(5), P. 499-513.
- [16] Abdallah B., Alnama K., Nasrallah F. Deposition of ZnS thin films by electron beam evaporation technique, effect of thickness on the crystallographic and optical properties. *Modern Physics Letters B*, 2019, **33**(04), P. 1950034.
- [17] Basak A., Hati A., Mondal A., Singh U.P., Taheruddin S.K. Effect of substrate on the structural, optical and electrical properties of SnS thin films grown by thermal evaporation method. *Thin Solid Films*, 2018, **645**, P. 97-101.
- [18] Abdallah B., Duquenne C., Besland M.P., Gautron E., Jouan P.Y., Tessier P.Y., et al. Thickness and substrate effects on AlN thin film growth at room temperature. *The European Physical Journal – Applied Physics*, 2008, **43**(3), P. 309-13.
- [19] Rahmane S., Abdallah B., Soussou A., Gautron E., Jouan P.-Y., Le Brizoual L., et al. Epitaxial growth of ZnO thin films on AlN substrates deposited at low temperature by magnetron sputtering. *physica status solidi (a)*, 2010, **207**(7), P. 1604-8.
- [20] Abdallah B., Rihawy M.S. Ion beam measurements for the investigation of TiN thin films deposited on different substrates by vacuum arc discharge. Nuclear Instruments and Methods in Physics Research Section B: Beam Interactions with Materials and Atoms, 2019, **441**, P. 33-40.
- [21] Al-Jawad SMH, Ismail MM. Characterization of Mn, Cu, and (Mn, Cu) co-doped ZnS nanoparticles. *J Opt Technol*. 2017;84(7):495-9.
- [22] Wu M., Zhiqiang W., Zhao W., Wang X., Jiang J. Optical and Magnetic Properties of Ni Doped ZnS Diluted Magnetic Semiconductors Synthesized by Hydrothermal Method. *Journal of Nanomaterials*, 2017, **2017**, P. 1-9.
- [23] Attaf A., Derbali A., Saidi H., Benamra H., Aida M.S., Attaf N., et al. Physical properties of Pb doped ZnS thin films prepared by ultrasonic spray technique. *Physics Letters A*, 2019, P. 126199.
- [24] Dixit N., Vaghasia J.V., Soni S.S., Sarkar M., Chavda M., Agrawal N., et al. Photocatalytic activity of Fe doped ZnS nanoparticles and carrier mediated ferromagnetism. *Journal of Environmental Chemical Engineering*, 2015, **3**(3), P. 1691-701.
- [25] Ahmad Z., Abdallah B. Controllability Analysis of Reactive Magnetron Sputtering Process. *Acta Physica Polonica A*, 2013, **123**, P. 3.
- [26] Altomare A., Corriero N., Cuocci C., Falcicchio A., Moliterni A., Rizzi R. QUALX2.0: a qualitative phase analysis software using the freely available database POW\_COD. *Journal of Applied Crystallography*, 2015, **48**(2), P. 598-603.
- [27] Toby B.H., Von Dreele R.B. GSAS-II: the genesis of a modern open-source all purpose crystallography software package. *Journal of Applied Crystallography*, 2013, **46**(2), P. 544-9.
- [28] Cheon J., Talaga D.S., Zink J.I. Photochemical Deposition of ZnS from the Gas Phase and Simultaneous Luminescence Detection of Photofragments from a Single-Source Precursor, Zn(S2COCHMe2)2. *Journal of the American Chemical Society*, 1997, **119**(1), P. 163-8.
- [29] Barreca D., Gasparotto A., Maragno C., Tondello E., Spalding T.R. Analysis of nanocrystalline ZnS thin films by XPS. *Surf Sci Spectra*. 2002, **9**, P. 51-64.
- [30] Burungale V., Devan R., Pawar S., Harale N., Patil V., Rao V., et al. Chemically synthesized PbS Nano particulate thin films for a rapid NO2 gas sensor. *MATERIALS SCIENCE-POLAND*, 2015, 34.
- [31] Zatsepin D.A., Boukhvalov D.W., Gavrilov N.V., Kurmaev E.Z., Zatsepin A.F., Cui L., et al. XPS-and-DFT analyses of the Pb 4f - Zn 3s and Pb 5d - O 2s overlapped ambiguity contributions to the final electronic structure of bulk and thin-film Pb-modulated zincite. *Applied Surface Science*, 2017, **405**, P. 129-36.
- [32] Langer D.W., Vesely C.J. Electronic Core Levels of Zinc Chalcogenides. *Physical Review B*, 1970, **2**(12), P. 4885-92.
- [33] Battistoni C., Paparazzo E., Dumond Y., Nogues M. X-ray photoelectron spectra of the spinel systems CdCr<sub>x</sub>In<sub>2-x</sub>S<sub>4</sub>. *Solid State Communications*, 1983, **46**(4), P. 333-6.

- [34] Barreca D., Tondello E., Lydon D., Spalding T.R., Fabrizio M. Single-Source Chemical Vapor Deposition of Zinc Sulfide-Based Thin Films from Zinc bis(O-ethylxanthate). *Chemical Vapor Deposition*, 2003, **9**(2), P. 93-8.
- [35] Briggs D. Handbook of X-ray Photoelectron Spectroscopy C.D. Wanger, W.M. Riggs, L.E. Davis, J.F. Moulder and G.E. Muilenberg Perkin-Elmer Corp., Physical Electronics Division, Eden Prairie, Minnesota, USA, 1979, **190**, P. 195. *Surface and Interface Analysis*, 1981, **3**(4).
- [36] Li Z., Liu B., Li X., Yu S., Wang L., Hou Y., et al. Synthesis of ZnS nanocrystals with controllable structure and morphology and their photoluminescence property. *Nanotechnology*, 2007, **18**(25), P. 255602.
- [37] Yao T. Zinc Oxide. In: Buschow KHJr, Cahn R.W., Flemings M.C., Ilshner B., Kramer E.J., Mahajan S., et al., editors. *Encyclopedia of Materials: Science and Technology*, 2001, P. 9883-7.
- [38] Karan N.S., Sarkar S., Sarma D.D., Kundu P., Ravishankar N., Pradhan N. Thermally Controlled Cyclic Insertion/Ejection of Dopant Ions and Reversible Zinc Blende/Wurtzite Phase Changes in ZnS Nanostructures. *Journal of the American Chemical Society*, 2011, **133**(6), P. 1666-9.
- [39] Joyce H.J., Wong-Leung J., Gao Q., Tan H.H., Jagadish C. Phase Perfection in Zinc Blende and Wurtzite III-V Nanowires Using Basic Growth Parameters. *Nano Letters*, 2010, **10**(3), P. 908-15.
- [40] D'Amico P., Calzolari A., Ruini A., Catellani A. New energy with ZnS: novel applications for a standard transparent compound. *Scientific Reports*, 2017, **7**(1), P. 16805.